

## Supporting Information

### Diatom-mimetic channeled mesoporous silica membranes: Self-organized formation of hierarchical porous framework

Riku Kitamura,<sup>a</sup> Hiroto Watanabe,<sup>b</sup> Shouichi Somekawa,<sup>b</sup> Yuto Ono,<sup>a</sup> Yuka Owari,<sup>a</sup> Yuya Oaki,<sup>a</sup> and Hiroaki Imai<sup>\*a</sup>

<sup>a</sup>*Department of Applied Chemistry, Faculty of Science and Technology, Keio University, 3-14-1 Hiyoshi, Kohoku-ku, Yokohama 223-8522, Japan.*

<sup>b</sup>*Tokyo Metropolitan Industrial Technology Research Institute, 2-4-10 Aomi, Koto-ku, Tokyo 135-0064, Japan.*

#### Contents

**Table S1.** The thickness, relative density, trapping efficiency and permeability rate for the standard mesoporous silica membrane with macrochannels and reference membranes fabricated by pelletizing the spherical mesoporous silica beads.

**Figure S1.** SEM images of a silica frustule of a diatom, *Aulacoseira nipponica*.

**Figure S2.** Photo and SEM image of a glass fiber substrate.

**Figure S3.** Schematic illustration of the detailed preparation procedure for mesoporous silica membrane having straight macrochannels.

**Figure S4.** Nitrogen adsorption and desorption isotherms of the standard mesoporous silica membrane having straight macrochannels.

**Figure S5.** SEM image of the top surface of the standard mesoporous silica membrane having straight macrochannels.

**Figure S6.** Photo and SEM images of the free-standing mesoporous silica membrane having straight macrochannels fabricated on the plastic sheets.

**Figure S7.** Nitrogen adsorption and desorption isotherm and pore size-distribution of mesopores in the silica wall of free-standing mesoporous silica membrane having straight macrochannels fabricated on the plastic sheets.

**Figure S8.** Small angle X-ray diffraction pattern of the standard mesoporous silica membrane having straight macrochannels with the glass fibre substrate.

**Figure S9.** SEM images of the silica membrane having straight macrochannels prepared on a silicon substrate.

**Figure S10.** SEM images, nitrogen adsorption and desorption isotherms, and pore-size distribution of standard spherical silica beads having straight microchannels.

**Figure S11.** Schematic illustration of the detailed preparation procedure for spherical silica beads having straight microchannels.

**Figure S12.** Side-view SEM images of straight macrochannels in the silica membranes prepared with various stirring times.

**Figure S13.** Top-view SEM images of straight macrochannels in the silica membranes prepared with various water/TEOS molar ratios.

**Figure S14.** Top-view SEM images of macrochannels in the spherical silica beads prepared with various surfactants.

**Figure S15.** SEM images and nitrogen adsorption and desorption isotherms of spherical silica beads fabricated without surfactants.

**Figure S16.** Schematic illustration of the detail experimental method for evaluation of the trapping rate of methylene blue permeation with filtration.

**Figure S17.** Side-view SEM images of straight macrochannels in the silica membranes prepared without and with liquid paraffin pre-treatment.

**Figure S18.** SEM image of the surface of a membrane fabricated by pelletizing the powdered spherical silica beads having straight macrochannels.

**Figure S19.** Ultraviolet-visible absorption spectrum and its Tauc plots of titanium dioxide nanoparticles produced in the standard mesoporous silica membrane having straight macrochannels.

**Figure S20.** STEM image and EDX profile of the powdered sample of the standard mesoporous silica membrane loaded with titanium dioxide nanoparticles.

**Figure S21.** SEM images of the powdered sample of the standard silica membrane loaded with titanium dioxide nanoparticles.

**Table S1.** The thickness, relative density, trapping efficiency, and permeability rate for the standard mesoporous silica membrane with macrochannels and references (Membrane A, B, and C) fabricated by pelletizing powder obtained with milling the channeled samples.

	Channeled membrane	Membrane A (Dense)	Membrane B (Medium)	Membrane C (Sparse)
Thickness ( $\mu\text{m}$ )	60*	59	65	89
Relative density ( $\text{g} \cdot \text{cm}^{-3}$ )	0.49	0.62	0.46	0.32
Trapping efficiency (%)	99.9	99.9	99.3	88.6
Permeability rate ( $\text{dm}^3 \cdot \text{min}^{-1} \cdot \text{cm}^{-2}$ )	8.9	0.33	1.9	8.2

\*The total thickness of the macrochannel layers on the front and back sides of the membrane.

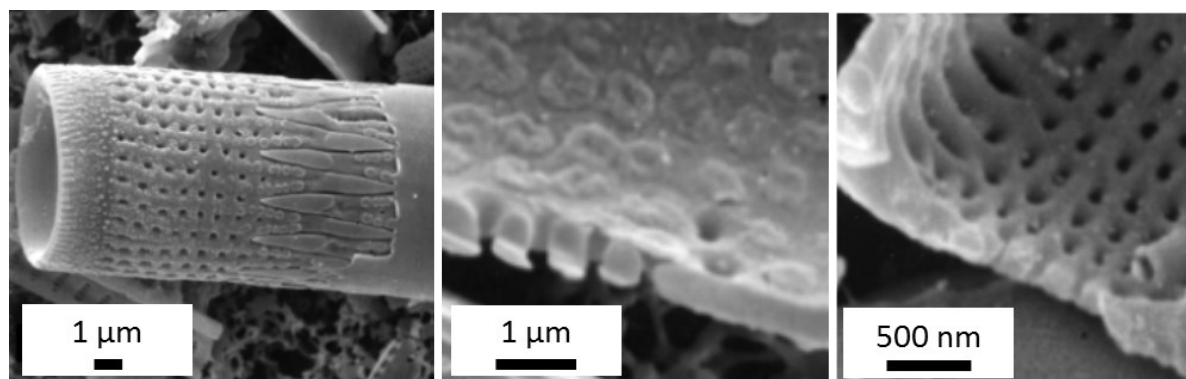


**Figure S1.** SEM images of a silica frustule of a diatom, *Aulacoseira nipponica*. Reproduced from ref. # S1 with permission by John Wiley and Sons.

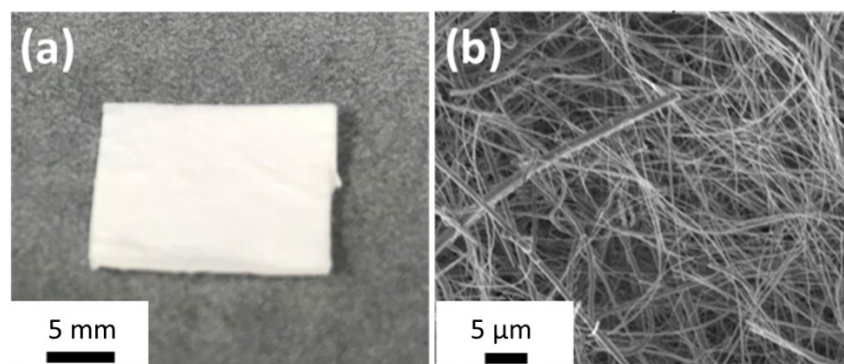
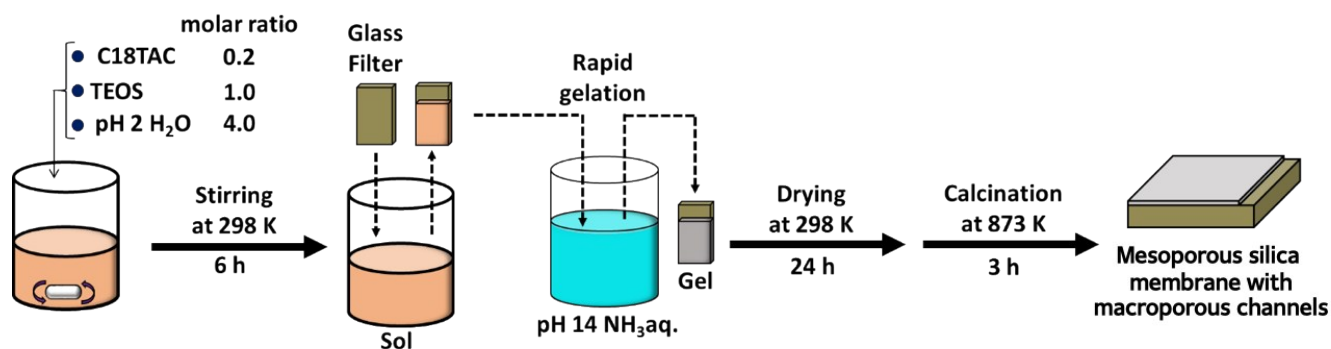


**Figure S2.** (a) Photo and (b) SEM image of a glass fiber substrate (Whatman GF/B).



□ □

**Figure S3.** Schematic illustration of the detailed preparation procedure for mesoporous silica membrane having straight microchannels. A concentrated silicate–surfactant solution was prepared by mixing TEOS, C18TAC, and H<sub>2</sub>O (hydrochloric acid, pH 2). The standard molar ratio of TEOS, H<sub>2</sub>O and C18TAC was 1.0 : 4.0 : 0.2. The mixed solution was stirred at 298 K for 6 h. We deposited the precursor solution (sol) on a glass fiber substrate ~500 μm thick (Whatman GF/B, Fig. S2) via a conventional dipping technique. The glass fiber substrate was then immersed in an ammonia solution at pH 14 to promote rapid polymerization of the silicate in the precursor solution deposited on the substrate. The gel film on the substrate was dried in air at 298 K for 24 h. We obtained micrometer-thick silica membranes on the substrate after calcination at 873 K in air. We prepared the macrochanneled membranes only on the glass fibre substrate to evaluate their properties. We dipped the glass fibre substrate in liquid paraffin to avoid the infiltration of the precursor solution into the densely tangled fibres. Thus, the macrochanneled membranes were formed on the substrate. Finally, the paraffin was removed during calcination after the formation of the membranes.

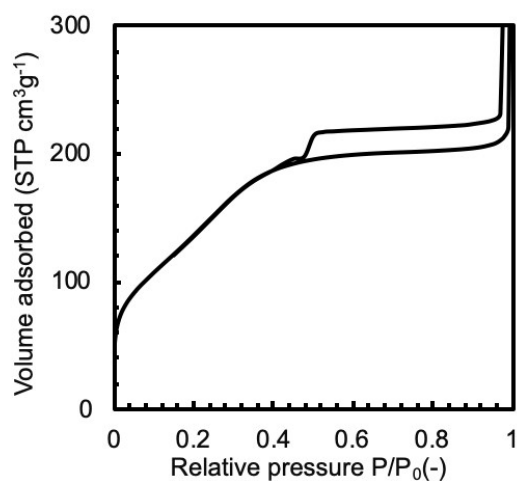


**Figure S4.** Nitrogen adsorption and desorption isotherms of the standard mesoporous silica membrane having straight macrochannels with the glass fiber substrate.

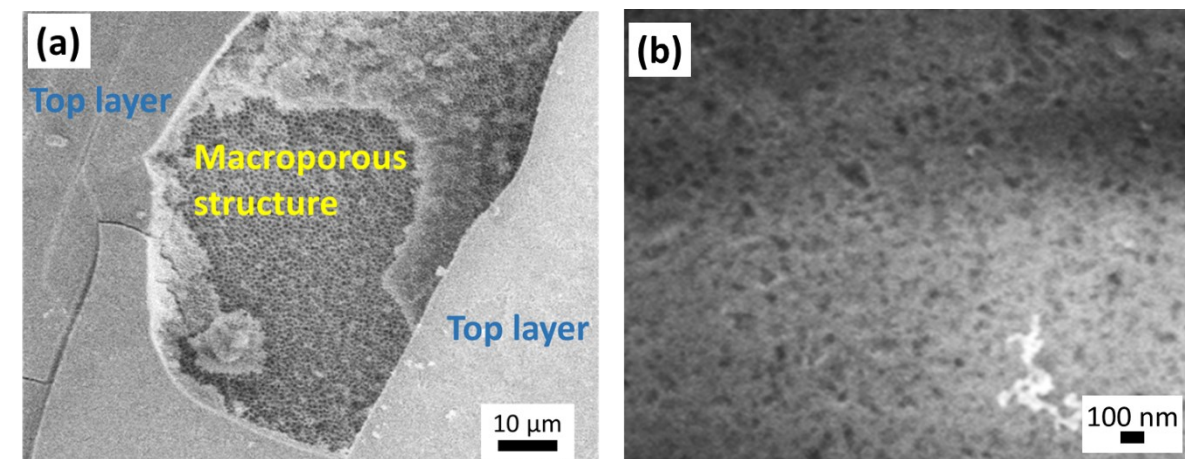


**Figure S5.** SEM images (a, b) of the top surface of the standard mesoporous silica membrane having straight macrochannels. The top layer was partially peeled off and the macrochannels were observed from the peeled area (a). We observed mesopore windows  $\sim 50$  nm in diameter on the magnified image of the top layer (b).

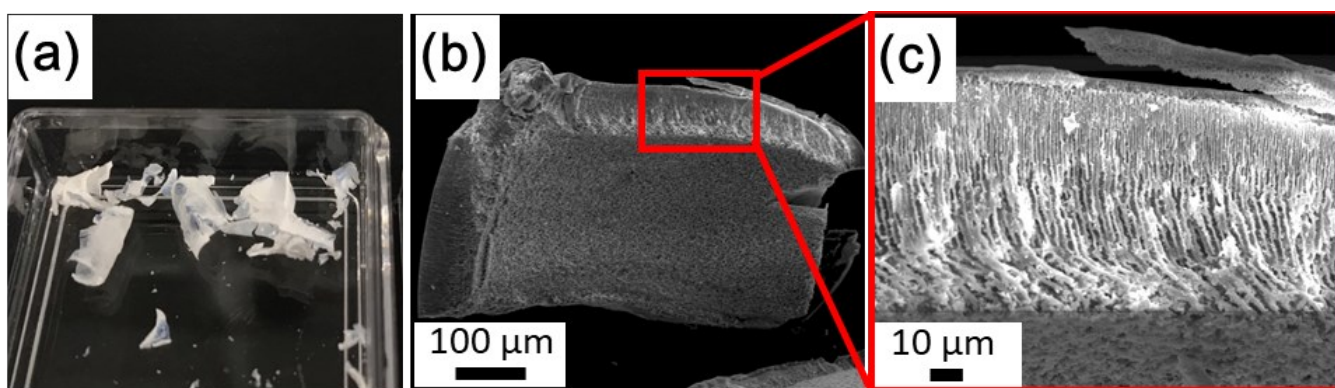


**Figure S6.** Photo (a) and SEM images (b, c) of the free-standing mesoporous silica membrane having straight macrochannels fabricated on the plastic sheets. The plastic sheets were removed after calcination at 873 K in air and free-standing films were obtained (a). We observed macrochannel structure in the films (b, c).

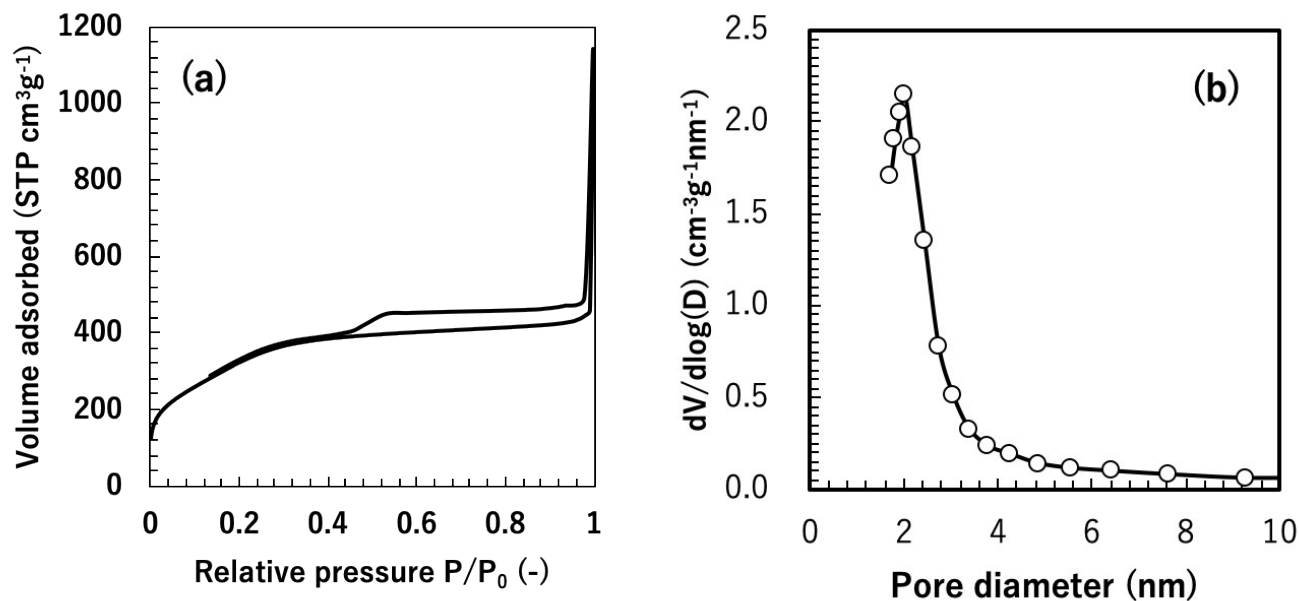


**Figure S7.** Nitrogen adsorption and desorption isotherm (a) and pore size-distribution of mesopores in the silica wall (Barrett-Joyner-Halenda (BJH) method) (b) of free-standing mesoporous silica membrane having straight macrochannels. BET specific surface area was estimated to be 1200 m<sup>2</sup>/g.

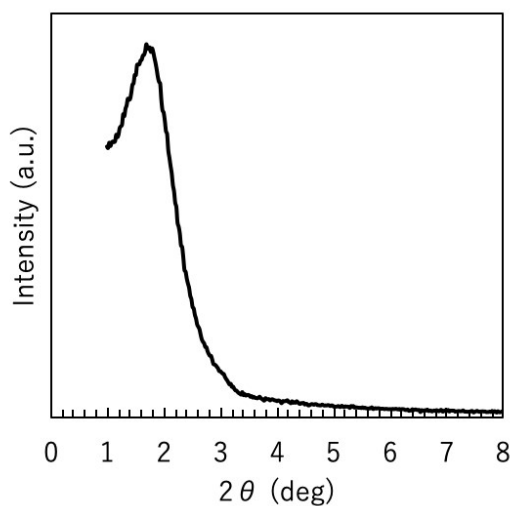


**Figure S8.** Small angle X-ray diffraction pattern of the standard mesoporous silica membrane having straight macrochannels with the glass fibre substrate.

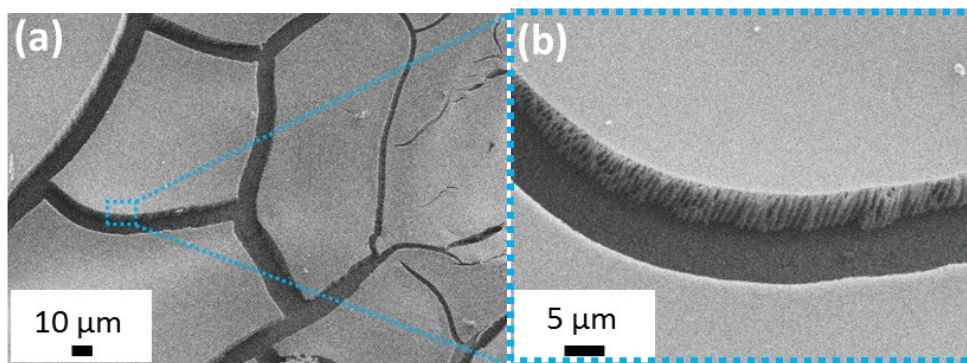


**Figure S9.** SEM images of a silica membrane having straight microchannels prepared on a silicon substrate. We observed many cracks due to the shrinkage of the membrane during the calcination process.

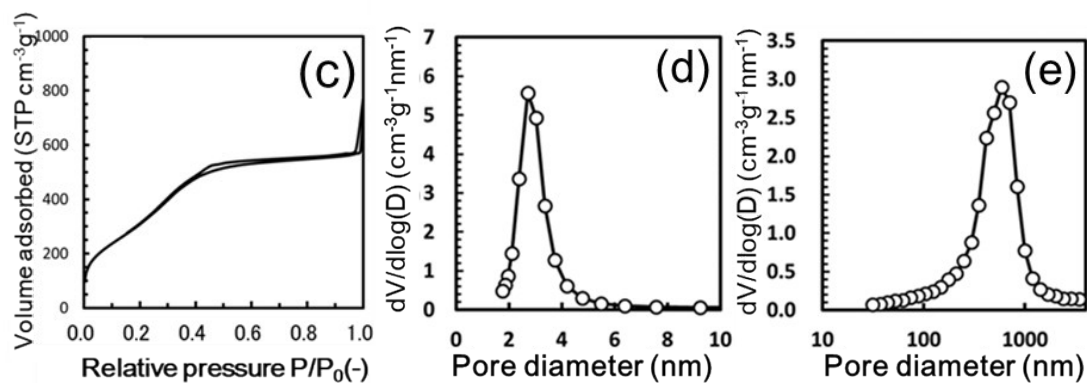
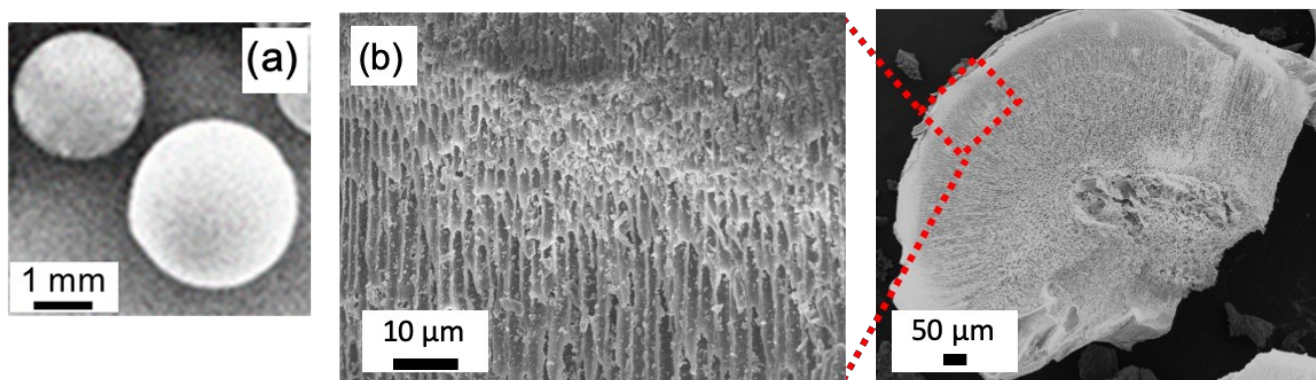


**Figure S10.** SEM images (a, b), nitrogen adsorption and desorption isotherms (c), and pore-size distribution estimated from the nitrogen adsorption isotherm (d) and mercury intrusion (e) of the standard spherical silica beads having straight macrochannels. The specific surface area was estimated to be  $\sim 1200$   $\text{m}^2/\text{g}$ .

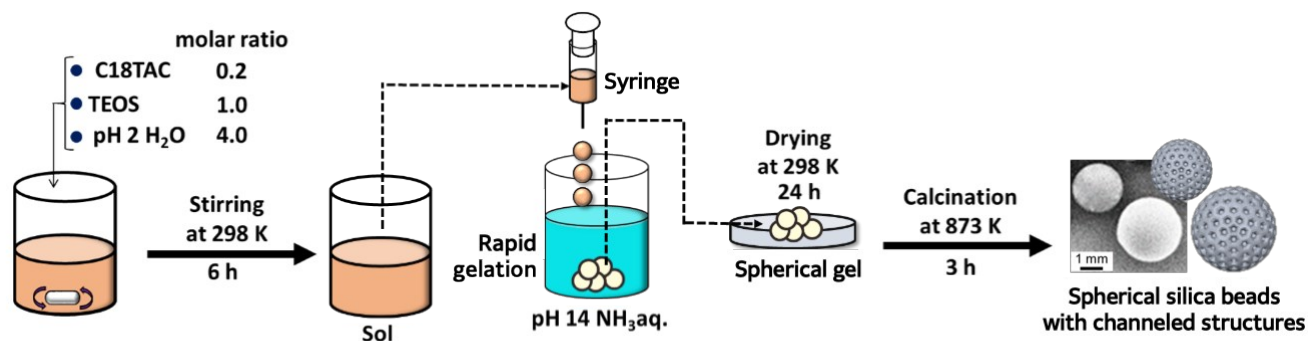


**Figure S11.** Schematic illustration of the detailed preparation procedure for spherical silica beads having macrochannels. A concentrated silicate-surfactant solution was prepared by mixing TEOS, C18TAC, and H<sub>2</sub>O (hydrochloric acid, pH 2.0). The standard molar ratio of TEOS, H<sub>2</sub>O and C18TAC was 1.0 : 4.0 : 0.2. The molar ratio of TEOS/water ratio was varied from 1 : 4 (standard) to 1 : 12. The mixed solution was stirred at 298 K. The stirring time was varied from 1 to 24 h, the standard stirring time was 6 h. We dropped the precursor solution (sol) into an ammonia solution at pH 14 with a syringe to promote rapid polymerization of the silicate in the precursor solution. The produced spherical gel beads (~1 mm) were dried in air at 298 K for 24 h. We obtained spherical silica beads with channeled structures after calcination at 873 K in air.

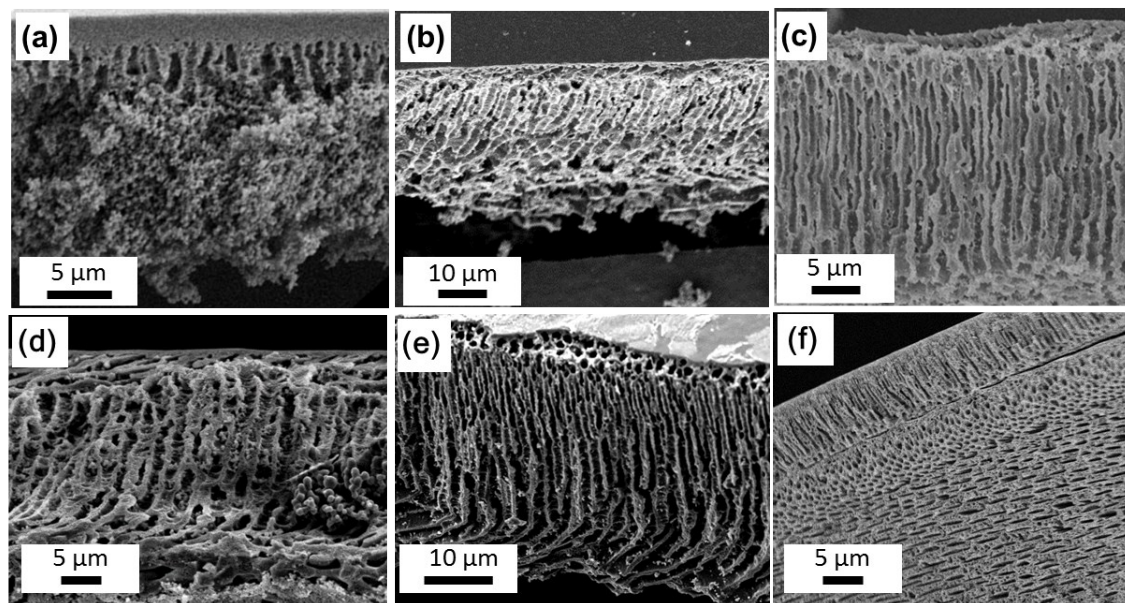


**Figure S12.** Side-view SEM images of straight macrochannels in the silica membranes prepared with various stirring times; 1 h (a), 3 h (b), 6 h (standard) (c), 12 h (d), 18 h (e), and 24 h (f).



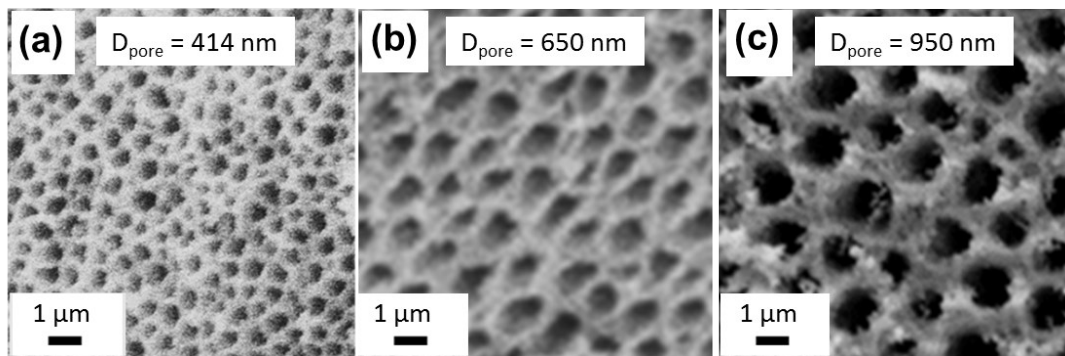


**Figure S13.** Top-view SEM images of macrochannels in the spherical silica beads prepared with various TEOS/water molar ratios; 1 : 4 (standard) (a), 1 : 10 (b), and 1 : 12 (c).

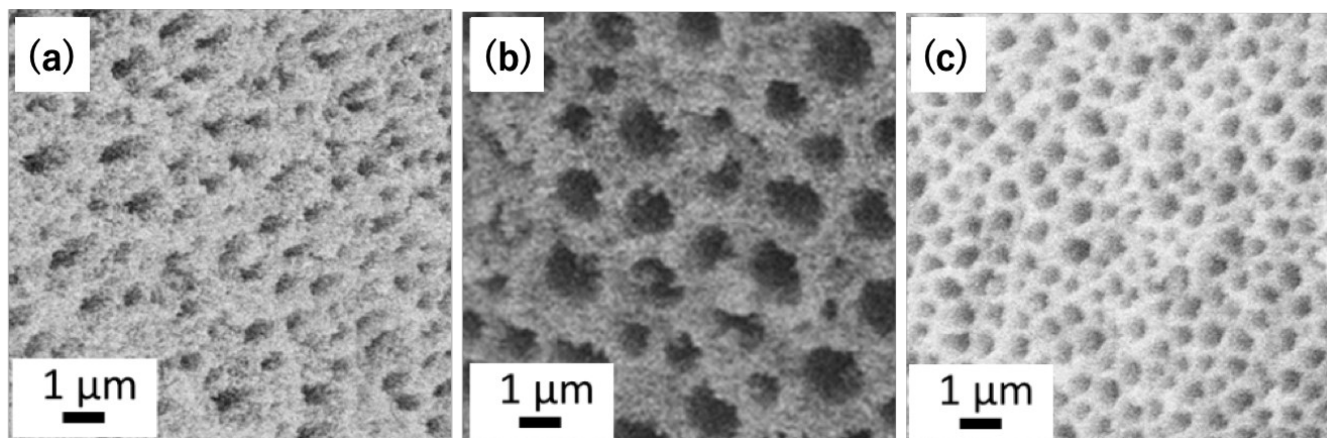


**Figure S14.** Top-view SEM images of macrochannels in the spherical silica beads prepared with various surfactants (a) C14TAC (b) C16TAC, and (c) C18TAC.

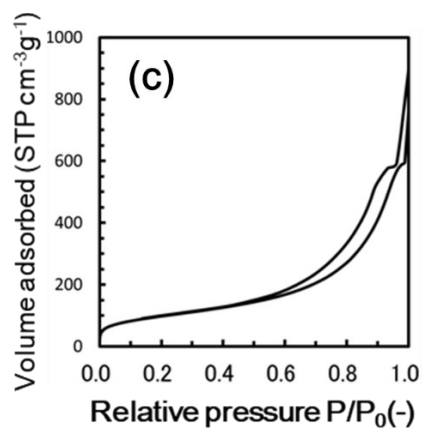
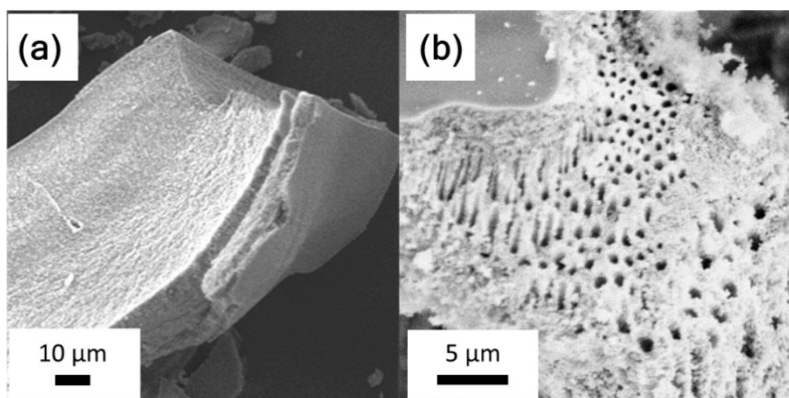


**Figure S15.** SEM images (a, b) and nitrogen adsorption and desorption isotherms (c) of spherical silica beads fabricated without surfactants. We obtained spherical silica beads without macrochannels (a). The channeled structures were partially found in the spherical silica beads (b). The isotherms indicate the absence of mesopores in the spherical silica beads.

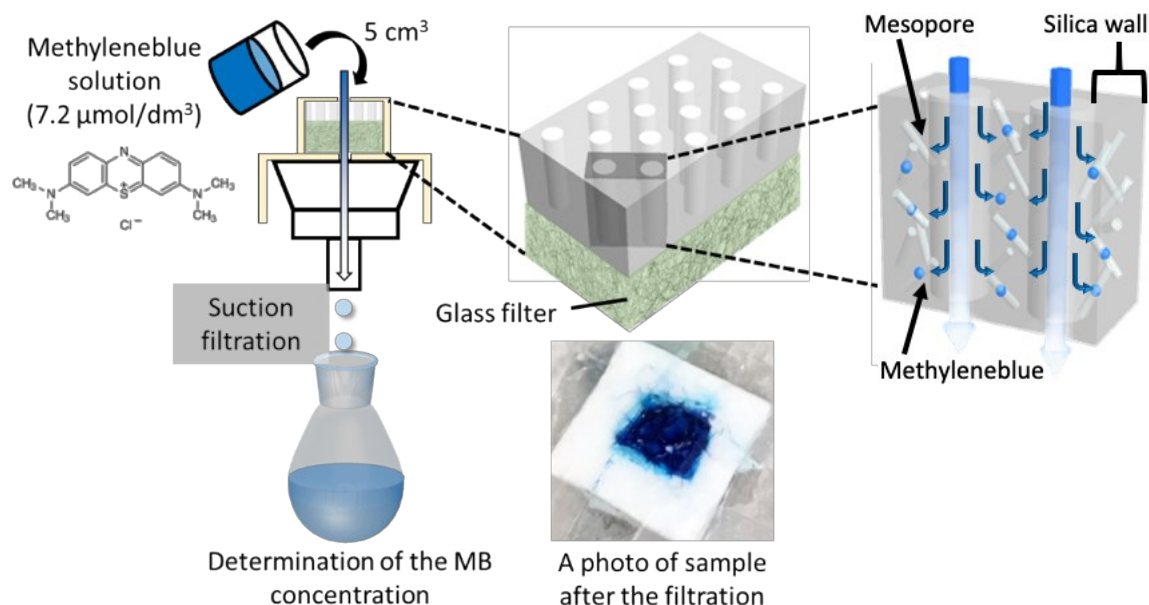


**Figure S16.** Schematic illustration of the detail experimental method for evaluation of trapping rate of methylene blue (MB) with filtration. An MB aqueous solution ( $7.2 \mu\text{mol}/\text{dm}^3$ ) was poured from the top of the membrane and permeated by suction filtration. The concentration of methylene blue was determined by ultraviolet-visible absorption spectra. The collection rates and the flow rates were measured during the experiments.

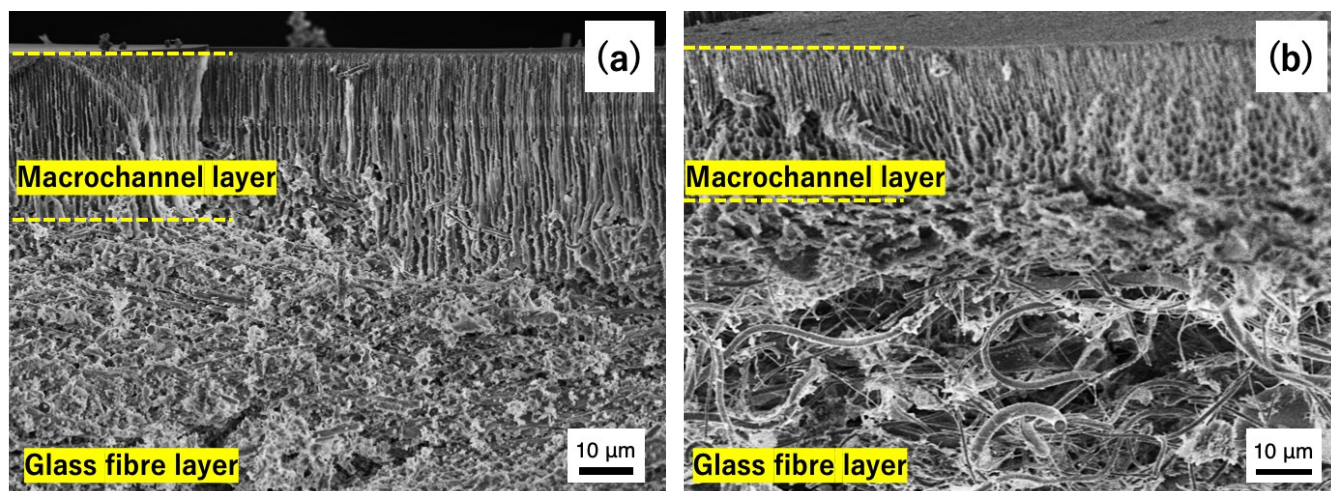


**Figure S17.** Side-view SEM images of straight macrochannels in the silica membranes prepared (a) without and (b) with liquid paraffin pre-treatment. By infiltrating a liquid paraffin in the glass fibre layer before depositing a precursor sol, only the macrochannel layer was formed on the surface of the glass fiber substrate (b).

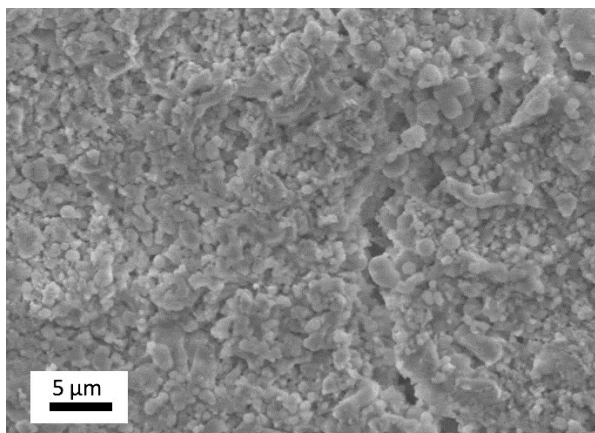


**Figure S18.** SEM image of the surface of a reference membrane fabricated by pelletizing the powdered spherical silica beads. The channeled structure was destroyed by milling with an agate mortar and a pestle.

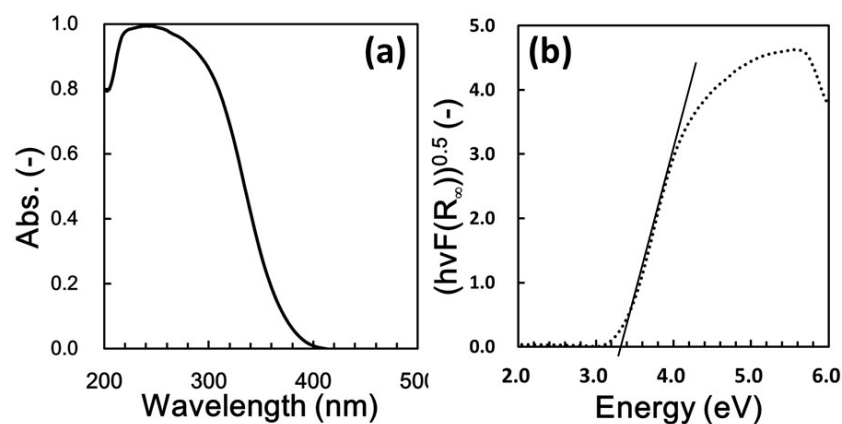


**Figure S19.** Ultraviolet-visible absorption spectrum (a) and its Tauc plots (b) of titanium dioxide nanoparticles produced in the standard mesoporous silica membrane having straight macrochannels.

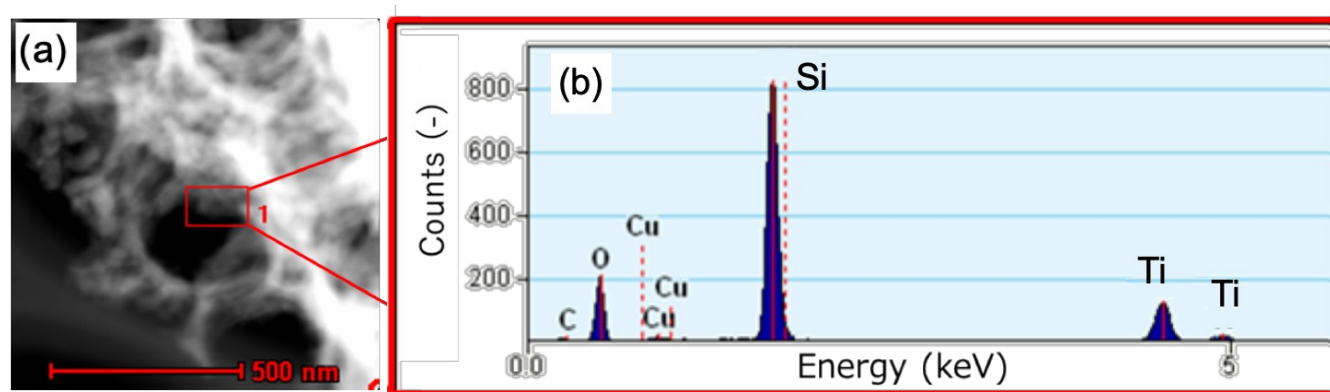


**Figure S20.** STEM image (a) and EDX profile (b) of the powdered sample of the standard mesoporous silica membrane loaded with titanium dioxide nanoparticles. Copper signals in the EDX profile are from

the copper grid.

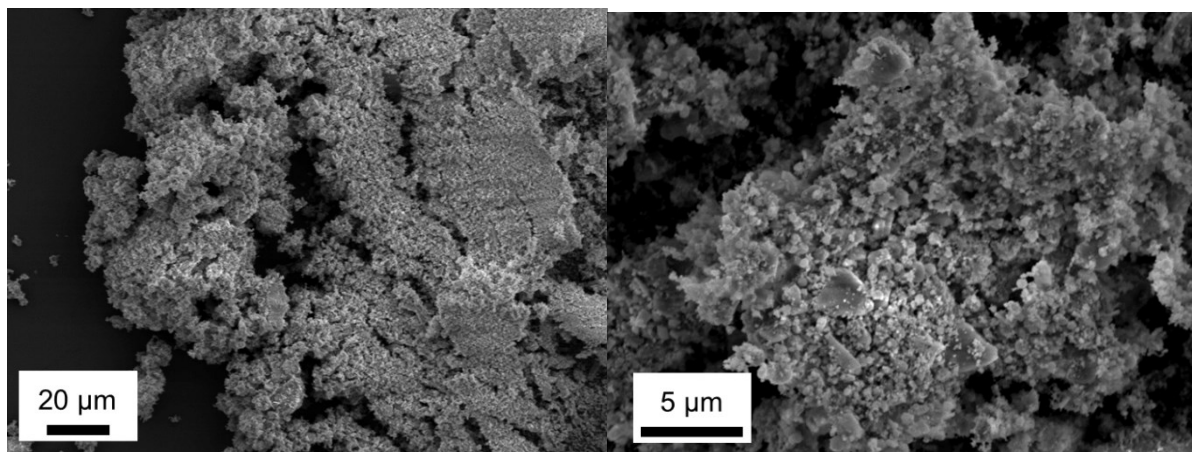


**Figure S21.** SEM images of the powdered sample of the standard mesoporous silica membrane loaded with titanium dioxide nanoparticles. The channeled structure was not observed after milling with an agate mortar and a pestle.

### Reference

S1. Y. Tanimura, M. Kato, H. Fukusawa, S. Mayama, K. Yokoyama, Cytoplasmic Masses Preserved in Early Holocene Diatoms: A Possible Taphonomic Process and its Paleo-Ecological Implications. *J. Phycol.* 2006, **42**, 270-279.